Contents lists available at ScienceDirect

Transactions of Nonferrous Metals Society of China

36(2026) 124−143

www.tnmsc.cn

Influence of interface shape on microstructure and mechanical properties of Mg/Al composite plates fabricated by hot-pressing

Shi-jun TAN [a], Bo SONG [a,*], Hao-hua XU [a], Ting-ting LIU [a,**], Jia SHE [b], Sheng-feng GUO [a], Xian-hua CHEN [b], Kai-hong ZHENG [c], Fu-sheng PAN [b]

[a] School of Materials and Energy, Southwest University, Chongqing 400715, China;
[b] College of Materials Science and Engineering, Chongqing University, Chongqing 400044, China;
[c] Institute of New Materials, Guangdong Academy of Science, Guangzhou 510650, China

Abstract: A new method was proposed for preparing AZ31/1060 composite plates with a corrugated interface, which involved cold-pressing a corrugated surface on the Al plate and then hot-pressing the assembled Mg/Al plate. The results show that cold-pressing produces intense plastic deformation near the corrugated surface of the Al plate, which promotes dynamic recrystallization of the Al substrate near the interface during the subsequent hot-pressing. In addition, the initial corrugation on the surface of the Al plate also changes the local stress state near the interface during hot pressing, which has a large effect on the texture components of the substrates near the corrugated interface. The construction of the corrugated interface can greatly enhance the shear strength by 2−4 times due to the increased contact area and the strong "mechanical gearing" effect. Moreover, the mechanical properties are largely depended on the orientation relationship between corrugated direction and loading direction.

Keywords: Mg/Al composite plate; interface shape; microstructure; mechanical properties; texture

1 Introduction

In the past few years, the use of lightweight and high-strength laminated metal composites (LMCs) has surged due to the expanding new energy vehicle market and the increasing demand for high-thrust spacecraft in the aerospace industry [1,2]. Multi-layer composite materials like Ti/Al [3], Ti/Mg [4], Al/Cu [5] and Mg/Al [6,7] etc., have been developed. Among these, the Mg/Al LMCs have garnered significant attention [6−8]. Mg and its alloys boast high specific stiffness, specific strength and exceptional damping performance as the lightest structural metal materials [9−12]. Conversely, Al and its alloys demonstrate excellent corrosion resistance and remarkable plastic formability [13,14]. Therefore, Mg/Al LMCs are anticipated to amalgamate the strengths of Mg alloys and Al alloys, thus widening their potential applications.

Mg/Al LMCs have been produced through various methods such as composite casting [15,16], explosive welding [17−19], diffusion bonding [20−22], and plastic processing bonding (e.g., hot-pressing [23,24], hot extrusion [25−30] and hot rolling [2,31−34]), etc. It is reported that achieving strong interface bonding for Mg/Al LMCs may be challenging due to their different physical and chemical properties [35,36]. The interface bonding strength comes mainly from two sources, i.e., metallurgical bonding and mechanical bonding [37]. Metallurgical bonding strength can be influenced by

Corresponding author: *Bo SONG, Tel: +86-23-68253204, E-mail: bosong@swu.edu.cn;
**Ting-ting LIU, Tel: +86-23-68253204, E-mail: ttliu@swu.edu.cn
https://doi.org/10.1016/S1003-6326(25)66953-6
Received 10 May 2024; accepted 20 January 2025

controlling the compositions and thickness of the diffusion layer [37]. For Mg/Al LMCs, the brittle Mg−Al intermetallic compounds are easy to form at the interface, which will largely deteriorate bonding strength [37]. The addition of an intermediate layer (e.g., zinc foil, silver foil, nickel foil and copper foil) at the Mg/Al interface can effectively change the structures and compositions of the diffusion layer and is proven to be highly effective in strengthening the metallurgical bonding [20,38−40]. Besides, the mechanical bonding strength can also be enhanced by tailoring the interface shapes. Explosive welding and CFR (corrugated roll/flat roll rolling + flat roll/flat roll rolling) roll-bonding can generate a corrugated interface in the Mg/Al LMCs [41]. Moreover, WANG et al [42] fabricated Al/Mg/Al LMCs with a trapezoidal-shaped interface by pre-wire cutting and subsequent multi-pass hot rolling. It has been confirmed that the three-dimensional (3D) interface exhibits higher mechanical bonding strength than the two-dimensional interface.

In this work, a new method is proposed to fabricate the Mg/Al LMCs with a corrugated interface. It involves cold-pressing a corrugated surface on the Al side and then hot-pressing the assembled Mg/Al plate. The microstructure evolution and interface features were investigated systematically. It is noted that the 3D interface often exhibits significant anisotropy. However, there has been less report in previous studies examining the effect of 3D interfaces on mechanical properties. Here, the influence of interface shape on mechanical properties was studied. Related mechanisms were discussed.

2 Experimental

The materials used in this study were a hot-extruded AZ31 Mg plate with a thickness of 3 mm and a rolled 1060 Al plate with a thickness of 3 mm. AZ31 and 1060 plates were cut into 40 mm (RD) × 15 mm (TD) × 3 mm (ND) plates by the electric spark wire cutting machine. Here, RD, TD and ND represent the rolling direction, transverse direction and normal direction of plate, respectively. The surface of the plate was polished with 1000# silicon carbide abrasive paper to remove the oxide layer. In this work, a steel mold with a corrugated surface was prepared. The waves in the horizontal direction have a peak−peak separation of about 4 mm and a peak−valley distance of approximately 2 mm, as shown in Fig. 1(a). Part 1060 plates were cold-pressed at room temperature by using the steel mold to generate a corrugated surface with a peak−valley distance of 2 mm. The directions of corrugation are set in two ways, i.e., the horizontal direction of corrugation is parallel to the RD (marked as HD), and the vertical direction of corrugation is parallel to the RD (marked as VD). Before hot-pressing, the AZ31 and the 1060 plates were put into the ultrasonic cleaner for cleaning for 10 min.

In this work, three types of assemblies were performed to prepare Mg/Al composite plates, as shown in Figs. 1(b−d). One is that both plates have a flat surface (named as flat−flat (FF) plate), as shown in Fig. 1(b). The other two types are that the AZ31 plate has a flat surface and the 1060 plate has a corrugated surface (flat−corrugated (FC) plate). According to the relationship between corrugated direction and the RD, the FC plates are marked as FC-HD plates and FC-VD plates, respectively (see Figs. 1(c, d)). Finally, three types of plates were laminated together by the hot-pressing process. Before hot-pressing, the two hot-pressing molds were first heated to 350 °C. The molds were then placed in contact with the Mg/Al sample and held for 10 min to allow heating of the sample. Finally, the Mg/Al composite plates were assembled and underwent a hot-pressing process with a thickness reduction of 40% at a speed of 2 mm/min.

The composite plates were analyzed for interface microstructure using scanning electron microscopy (SEM) with an energy dispersive spectrometer (EDS). The microstructure was characterized using electron backscatter diffraction (EBSD, NordlysMax3 equipped). For SEM analysis, the samples were ground and then subjected to ultrasonic cleaning for 10 min. The AZ31 and 1060 substrates for EBSD measurement were ground and then electropolished with AC-2 solution and a solution of 10% perchloric acid and 90% absolute ethanol, respectively. Tensile tests along the RD were conducted using a material test machine. The tensile specimens with a dimension of 15 mm (RD) × 3 mm (TD) × 3.6 mm (ND) were cut from the plates. The room temperature tensile tests were carried out at a constant strain rate of $1\times10^{-3}\ s^{-1}$. The shear properties were evaluated by a previously reported methodology [35,38], as depicted in Fig. 2(a). Figure 2(b) illustrates the schematics of longitudinal

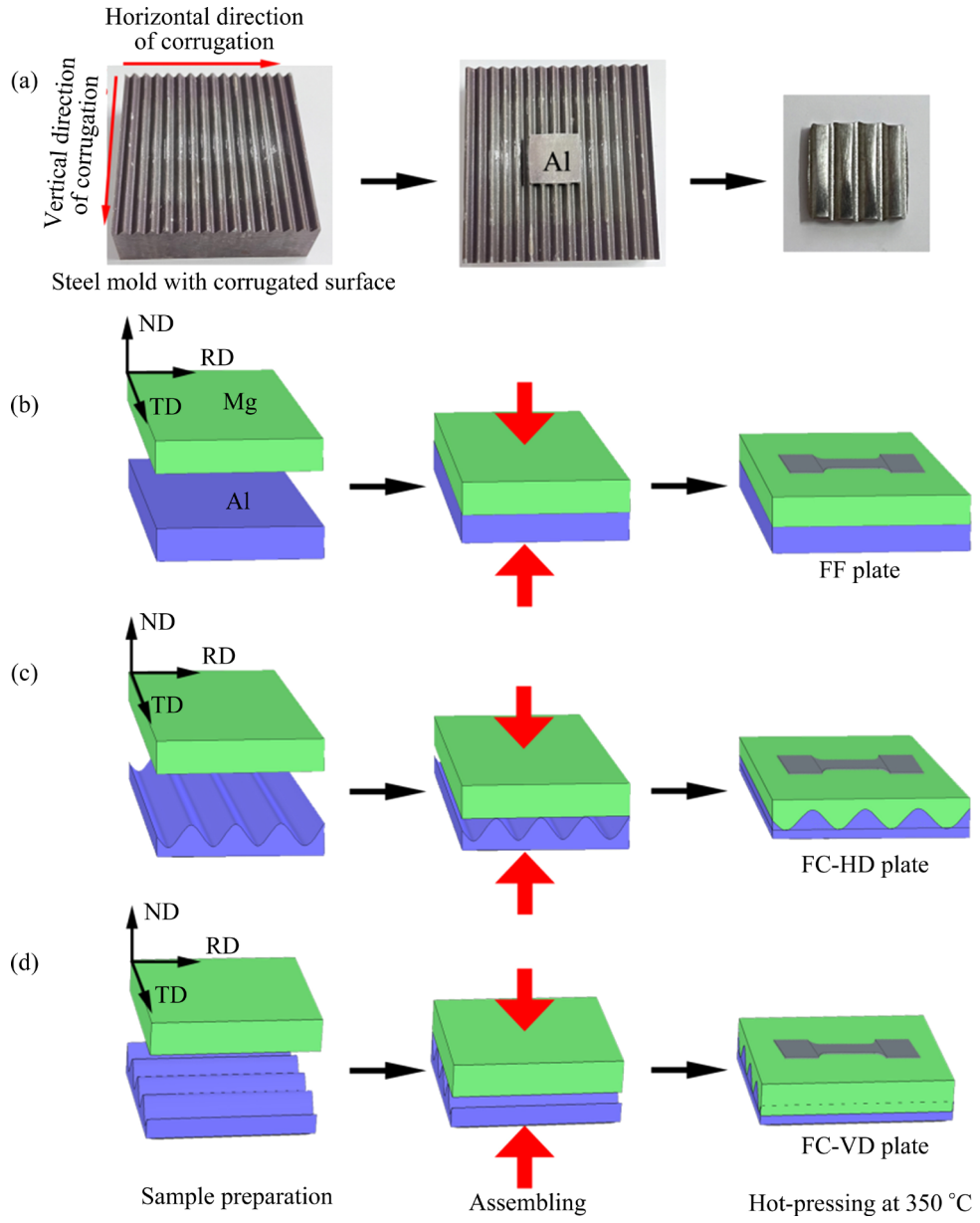

Fig. 1 (a) Steel mold with corrugated surface and fabrication of Al plate with corrugated surface; Processing schematic diagrams of (b) FF plate, (c) FC-HD plate and (d) FC-VD plate (The orientation of tensile sample is also marked)

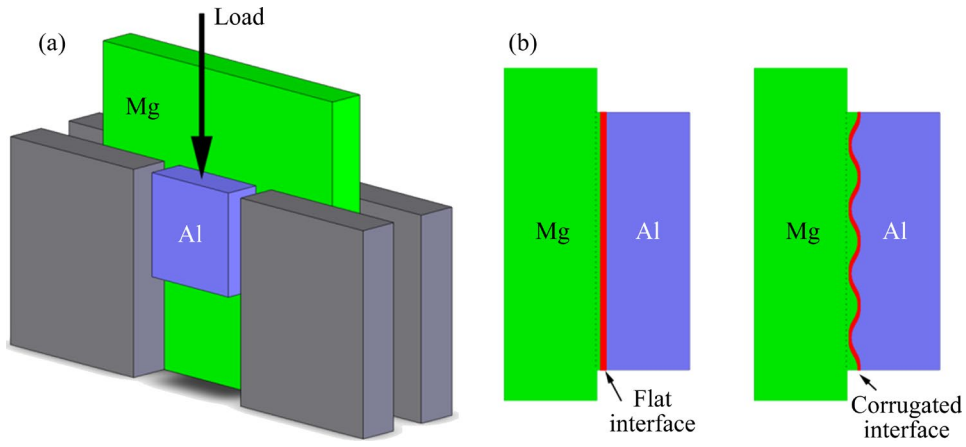

Fig. 2 (a) Test method of shear property and (b) schematic diagram of shear samples

sections of shear samples. In this study, the shear samples contained three corrugation cycles at the interface. Shear tests were performed at a loading speed of 1 N/s. Each set of experiments was repeated at least three times.

3 Results

3.1 Initial microstructure

Figure 3(a) shows the EBSD maps and the pole figures of the initial AZ31 plate. EBSD maps indicate that the AZ31 plate displays a mixed grain structure, i.e., both equiaxed fine-grains and elongated coarse-grains. Compared with equiaxed fine-grains, the elongated coarse-grains have higher KAM values and are therefore considered as the deformed grains. The IPF map shows that the *c*-axes of most grains (whether deformed grains or recrystallized grains) are concentrated in the ND. Thus, the initial AZ31 plate has a strong basal texture (see basal pole figure).

For the initial 1060 plate, most of the grains exhibit elongated grains. In order to better assess the morphological characteristics of elongated grains, EBSD maps on ND−TD plane and ND−RD plane were characterized, as shown in Figs. 3(b, c). For the elongated grains, major and minor axes of the ellipse usually correspond to the TD (RD) and the ND, respectively. According to the line intercept method, average grain sizes are 17.1, 14.3 and 9.0 μm along RD, TD and ND, respectively. The average aspect ratio (R) of elongated grains was also calculated by the ratio of major axis to minor axis. The R values are 1.9 and 1.6 on the ND−RD plane and ND−TD plane, respectively. The elongated grains have an average KAM value of ~1.00°. It is well known that the texture of hot-rolled pure Al usually consists of two main components: the cube component and β-fiber rolling orientations [43]. The cube component is the predominant texture observed in recrystallized grains, while the rolling orientations dominate in the deformed grains [44]. Pole figures indicate that the dominant component is cube {001}⟨100⟩ texture component, as shown in Figs. 3(b, c). Thus, as-received 1060 plate has a typical recrystallization texture.

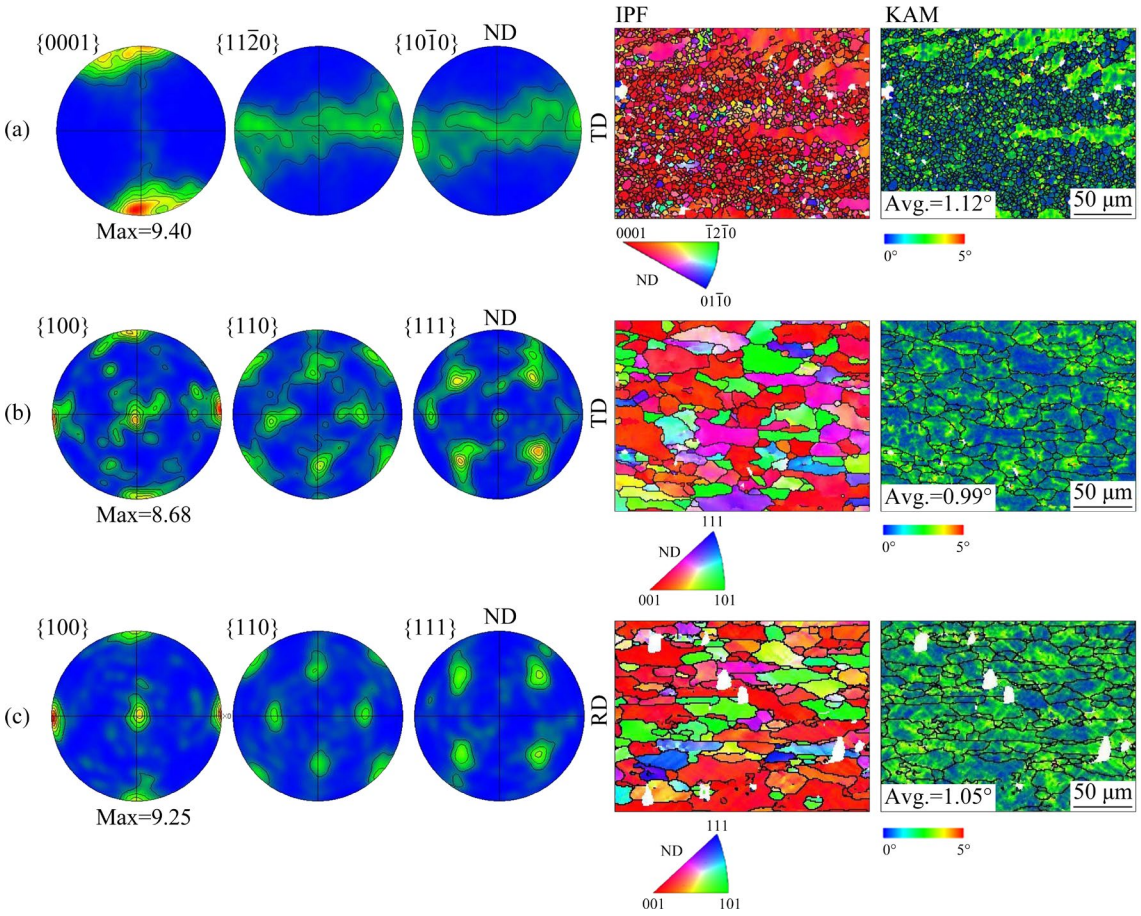

Fig. 3 Pole figures and EBSD maps of (a) ND−TD plane of initial AZ31 plate, (b) ND−TD plane of initial 1060 plate and (c) ND−RD plane of initial 1060 plate

3.2 Microstructure evolution during hot-pressing

Figure 4 shows the EBSD data of the ND−TD plane in the FF plate. For the Mg-layer, hot-pressing with a thickness reduction of 40% at 350 °C seems to increase the area fraction of equiaxed fine-grains, as shown in Fig. 4(a). In order to quantitatively assess the effect of hot-pressing on the microstructure of Mg-layer, the grain size distributions of initial AZ31 plate and the Mg-layer in the FF plate are shown in Figs. 5(a, b), respectively. The equiaxed fine-grains are typically less than 10 μm in grain size and have a low average KAM value (KAM<1°) for both samples. Thus, it is considered that they are the dynamic recrystallized grains. Hot-pressing increases the area fraction (f) of equiaxed fine-grains (<10 μm) from 75% to 93%, and slightly decreases the average grain size (d) of equiaxed fine-grains from 3.7 to 3.1 μm. Moreover, hot-pressing also reduces the average KAM value from 1.12° to 0.82° (see Figs. 3(a) and 4(a)). This indicates that hot-pressing induces the dynamic recrystallization process, resulting in the refinement of grains [45]. Moreover, after hot-pressing, typical basal texture can be maintained. The dynamic recrystallization can generate fine grains with different orientations [46]. Thus, compared with the initial sample, the pole intensity slightly decreases and the {0001} pole exhibits more scatter distribution (see the pole figure in Fig. 4(a)).

For the Al-layer, hot-pressing can also reduce

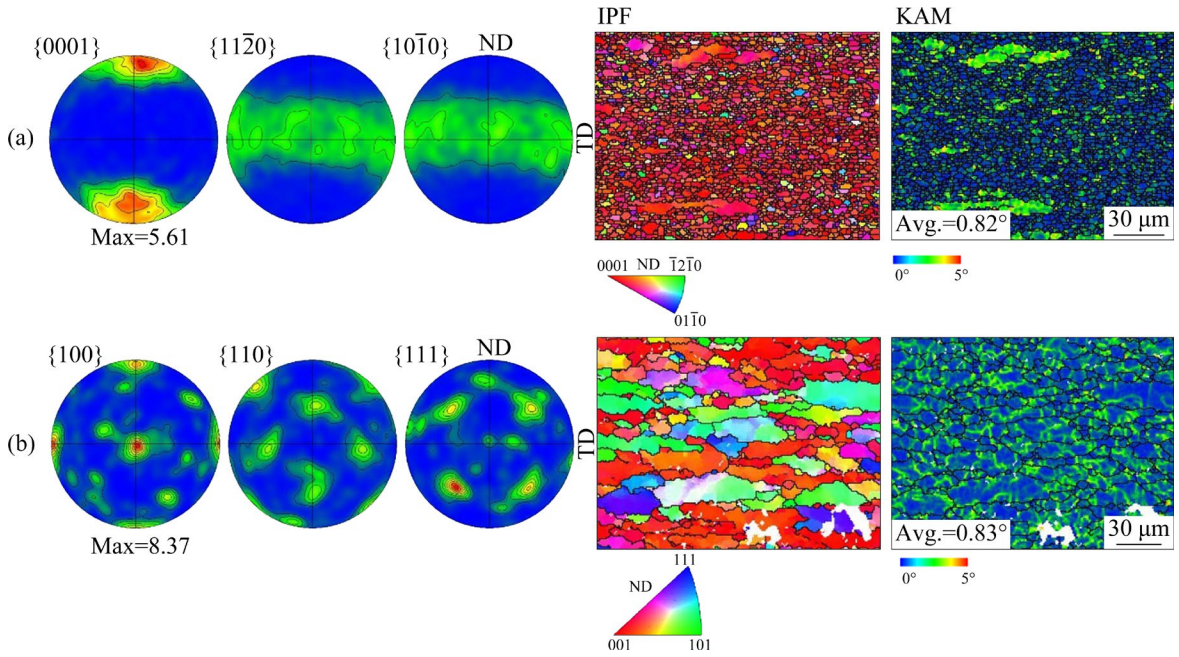

Fig. 4 Pole figures and EBSD maps of (a) ND−TD plane of FF-AZ31 plate and (b) ND−TD plane of FF-1060 plate

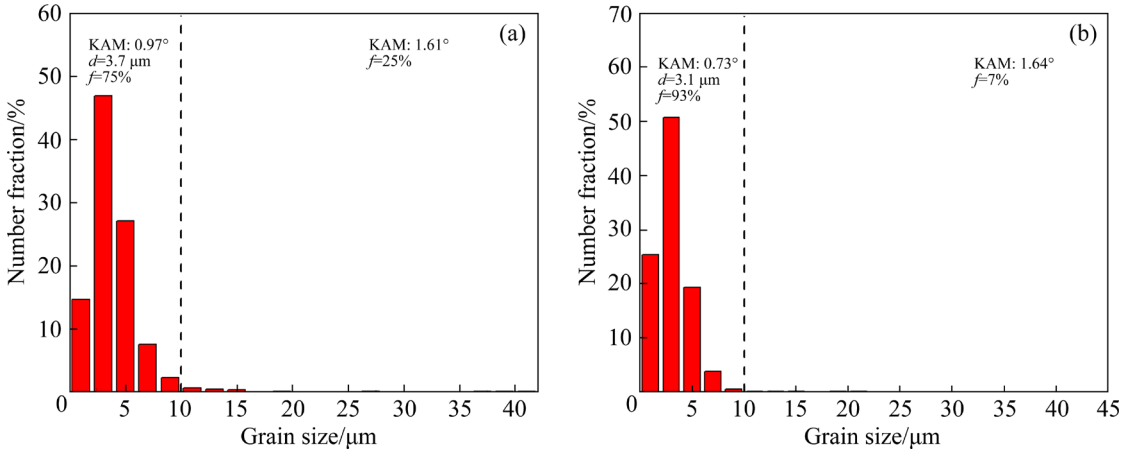

Fig. 5 Grain size distributions of (a) initial AZ31 plate and (b) AZ31 layer in FF plate (The grain size is the diameter of the equivalent circle)

the average KAM value and grain size, as shown Fig. 4(b). According to line intercept method, average major and minor axes on the ND−TD plane are 11.2 and 8.0 μm (R=1.4), respectively. After hot-pressing, the grain boundary exhibits a distinct wavy shape. This characteristic is commonly observed in the process of the discontinuous dynamic recrystallization. Moreover, the KAM map shows that the banded regions with high KAM values divides the grain into several cell-like regions with low KAM values. These results demonstrate that the hot-pressing can also initiate dynamic recrystallization in the Al layer. Clearly, present hot-pressing cannot cause profuse dynamic recrystallization in the Al alloy.

For the FC-HD plate and FC-VD plate, the relationship between corrugated direction and the RD is different, as shown in Fig. 1. This may affect the texture evolution during hot-pressing. However, the initial AZ31 plate has a typical basal texture (c-axis//ND) and their a-axes randomly rotate around the ND, as shown in Fig. 3(a). The initial 1060 plate has a typical cubic texture ({100}⟨001⟩ texture), as shown in Fig. 3(b). In other words, for initial 1060 plate, the ⟨100⟩ axis is parallel to both the RD and the TD. Thus, it is considered that the texture of the FC-HD and FC-VD plates shows similar textural changes during hot-pressing. Here, the ND−TD plane of the FC−VD plate is selected to analyze the microstructure evolution during the hot-pressing process.

Figure 6 shows the SEM images of the interface on the ND−TD plane of the FC−VD plate. After the hot-pressing, a corrugated interface is formed. The distance between adjacent wave valleys is approximately 5 mm. And there is a plateau with a length of ~1 mm between the two corrugations. The formation of the platform is caused by the plastic deformation of the wave peak on the 1060 surface during the hot-pressing process. The microstructure of typical positions was characterized by EBSD to examine the microstructure evolution. The typical positions include the wave peak (WP) position near the platform, the wave valley region (WV), the midpoint position between the wave peak and wave valley (WB) and the position which is away from waveform (AFW), as shown in Fig. 6. For the WB-R and WB-L positions, R and L represent the right and left sides, respectively.

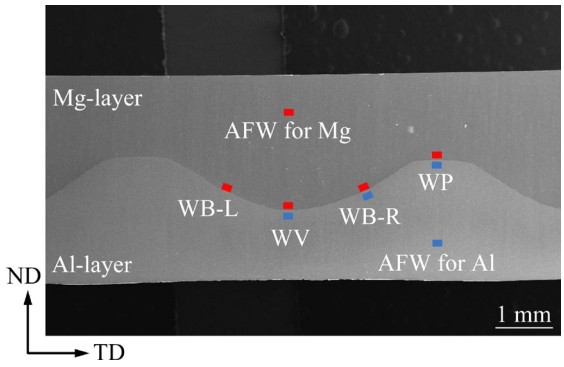

Fig. 6 SEM image of interface in FC-VD plate

Figure 7 shows the EBSD maps and {0001} pole figures of the Mg-layer on the ND−TD plane of the FC-VD plate. For the AFW, WP and WV positions, the long-axis direction of elongated grains is parallel to the TD and the c-axis of texture is still close to the ND (see Figs. 7(a, b, d)). However, for the WB (WB-R/WB-L) positions, the long axis of the elongated grains is nearly parallel to the inclined

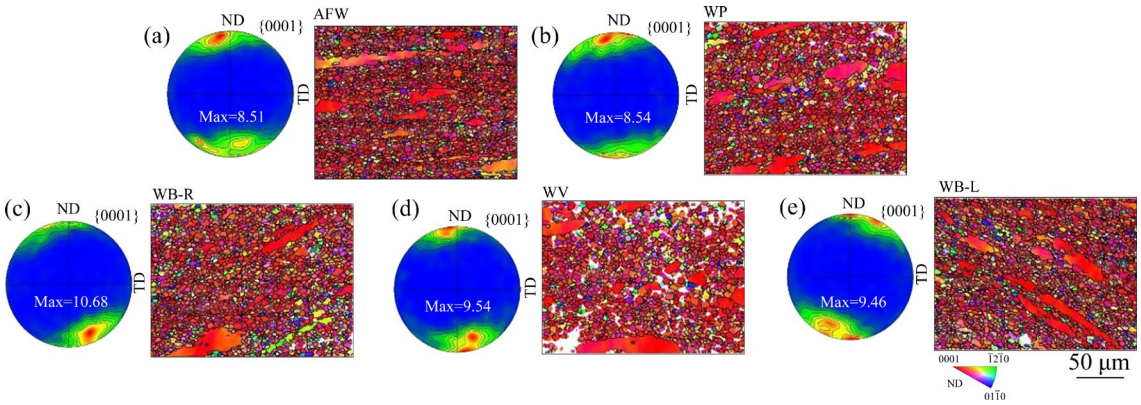

Fig. 7 EBSD maps of Mg-layer at various positions of FC-VD plate: (a) AFW position; (b) WP position; (c) WB-R position; (d) WV position; (e) WB-L position

interface. Moreover, the *c*-axis of texture is rotated towards the normal direction of the corrugated interface (see Figs. 7(c, e)). It is reported that the formation of texture in AZ31 alloys is largely dependent on the stress state during deformation [47]. Clearly, the initial corrugated surface on the Al matrix might change the local stress state in the WB positions of Mg matrix. The grain size distributions of various positions in the Mg matrix are shown in Figs. 8(a−d). Similar to the initial AZ31 plate and FF plate, equiaxed fine-grains have low KAM values (<0.83°). Hot-pressing can increase the area fraction of equiaxed fine-grains in the WB, WP and AFW positions (to >85%), but it exhibits little influence on that in the WV position.

Figure 9 shows the EBSD maps and pole figures of the Al-layer on the ND−TD plane of the FC-VD plate. The microstructure of the AFW position is similar to that of the FF plate, i.e., the long-axis direction of elongated grains is parallel to the TD (R=1.5 on the ND−TD plane), as shown in Fig. 9(a). In contrast, WP and WV positions contain more equiaxed grains (see Figs. 9(b, d)). The R is 1.3 and 1.2 on the ND−TD plane for WP and WV positions, respectively. The main texture component is still a cube component in the WP, WV and AFW positions. And the {100} texture of the WV position is more scattered than that in the other two positions. For the WB-R position, the shape of all grains changes from elongated to equiaxed (R=1.1), as shown in Fig. 9(c). The {001} plane tends to rotate from the ND towards the inclined interface around the RD, and texture components become more scattered, resulting in a low texture intensity. KAM maps indicate that hot-pressing exhibits little influence on the average KAM value for all positions in the Al substrate.

3.3 Interface structure of hot-pressed plates

Figure 10(a) shows the SEM image and EDS mappings of the FF plate. The SEM image shows that the Mg/Al plate interface is well bonded and no obvious defects (e.g., cracks, and voids) are present. This suggests that direct hot-pressing in an atmospheric environment can create effective bonding at the interface of the AZ31 plate and 1060

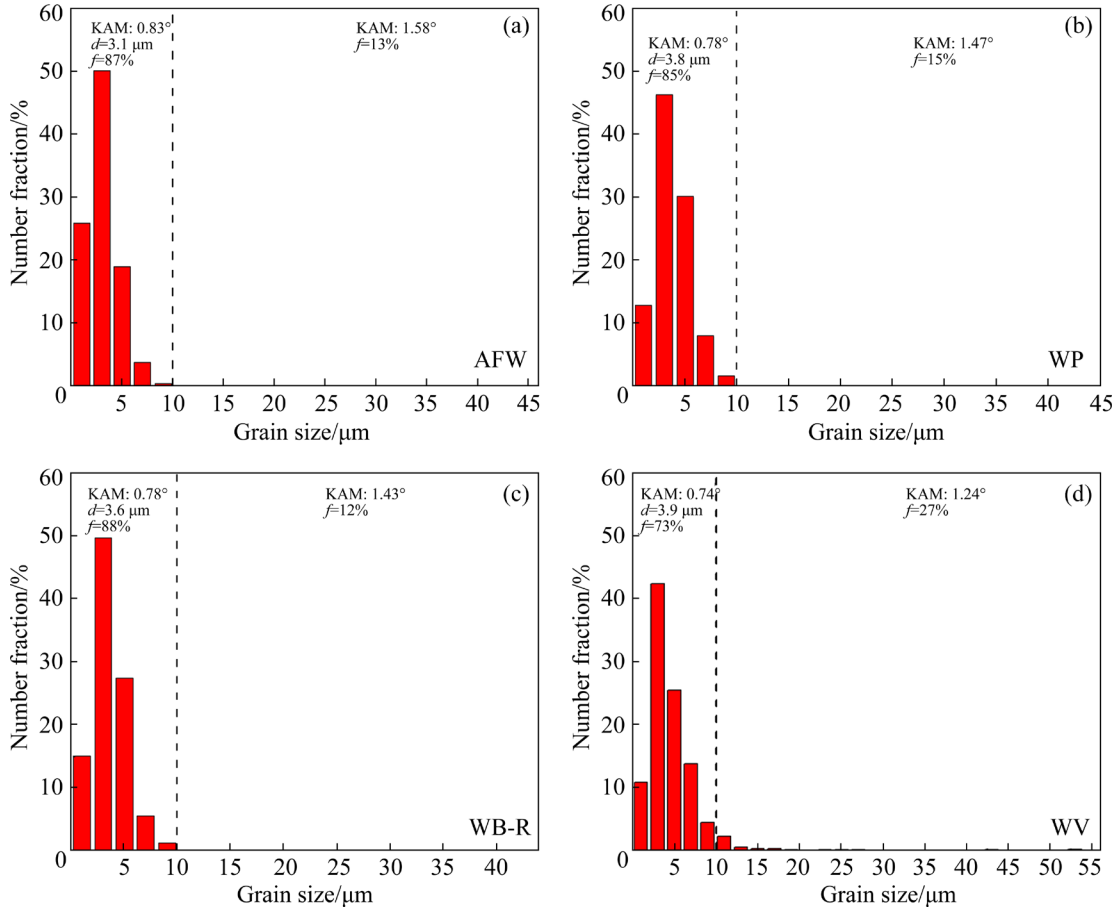

Fig. 8 Grain size distributions of AZ31 side at various positions of FC-VD plate: (a) AFW position; (b) WP position; (c) WB-R position; (d) WV position (The grain size is the diameter of the equivalent circle)

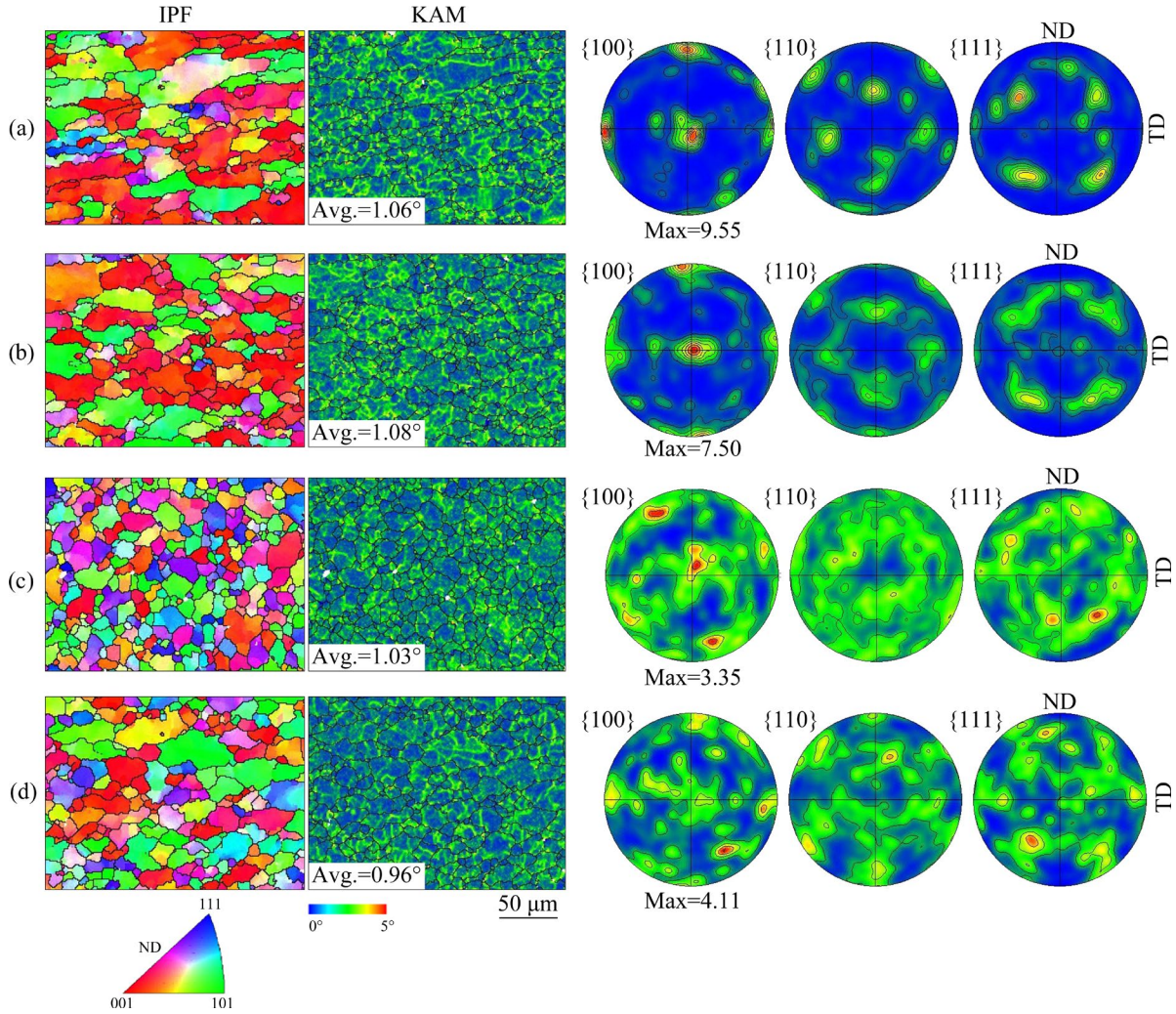

Fig. 9 EBSD maps of Al-layer at various positions of FC-VD plate: (a) AFW position; (b) WP position; (c) WB-R position; (d) WV position

plate. It has been reported that the occurrence of plastic deformation can generate more fresh surfaces to facilitate subsequent diffusion joining [48]. After hot-pressing, a distinct transition layer between two substrates can be found. Both the face-scan and line-scan plots show that an apparent interaction diffusion of elements is produced at the transition layer, as shown in Figs. 10(a, b). This proves that direct hot-pressing generates obvious metallurgical bonding at the interface of Mg/Al composite plate. According to the result of the EDS line-scan, the diffusion layer thickness (DLT) is ~5 μm, as shown in Fig. 10(b). This is similar to that of Mg/Al composite plates fabricated by hot rolling with reduction of 40% at 350 °C (~5 μm) [37].

According to the Mg−Al binary phase diagram [22], the maximum solid solubility of Mg in Al is ~10 at.% and that of Al in Mg is ~5 at.%, when the temperature is 350 °C. Therefore, the Mg−Al intermetallic compounds are inevitably formed during the diffusion bonding process. It has been reported that the diffusion layer in the diffusion-bonded Mg/Al composite plate contains Mg (ss)−reactive layer (γ-$Al_{12}Mg_{17}$ layer + β-Al_3Mg_2 layer)−Al (ss) [1]. The Mg-to-Al atomic ratios of the γ phase and β phase are ~1.42 and ~0.67, respectively. In order to further reveal the formation of intermetallic compounds, the zoomed-in line-scan plots in the region of the diffusion layer and the corresponding Mg-to-Al atomic ratio are shown in Fig. 10(c). In the vicinity of the matrix, the atomic ratio exhibits a continuous change. These zones may be single-phase solid solution zones or multiphase mixed zones. In addition, there is a compound layer with a relatively constant Mg-to-Al atomic ratio of ~0.75 adjacent to the Al matrix. The stoichiometric proportion is close

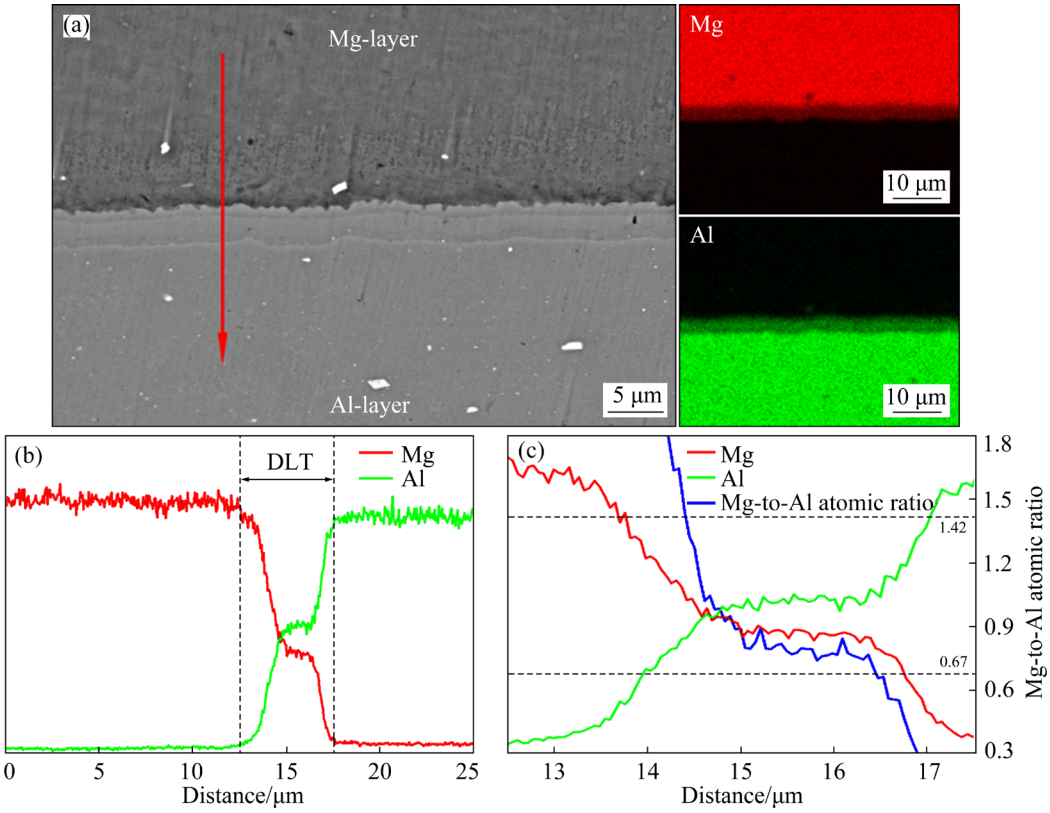

Fig. 10 (a) SEM image and EDS mappings of bonding interface on ND−TD plane of FF sample, (b) corresponding element line-canning spectrum and (c) zoomed-in line-scan plots in region of diffusion layer and corresponding Mg-to-Al atomic ratio

to the β phase. This infers that the single-phase region of β phase with size of ~1.5 μm can be formed adjacent to the Al matrix. However, no significant single-phase region of γ phase is observed in the diffusion region. In fact, this phenomenon is also similar to earlier report [32]. It has been reported that the activation energy of β phase is lower than that of γ phase. Thus, the growth constant of β phase is larger than that of γ phase [32].

Figure 11 shows the SEM images on the ND−TD plane of the FC-VD plate. For the FC plate with the corrugated interface, contact time, strain amount and the defect density of the matrix at different positions of the corrugated interface are different. It has been reported that these may affect the width of the diffusion layer [32,37]. Thus, three typical positions at the corrugated interface were characterized, as shown in Figs. 11(a−c). Overall, the entire corrugated interface is well-bonded. The EDS mappings show that Mg and Al elements are almost included in the whole interface, which indicates that there is a clear inter-diffusion of elements at the transition layer after hot-pressing. Based on the line scan data, it can be seen that the diffusion layer thickness is about 5 μm for three positions. Diffusion layer thickness does not vary much across the corrugated interface. Moreover, the variations of atomic ratio within the diffusion zone at different locations of the FC-VD plate are also shown in Fig. 11. Based on the above discussion, it can be inferred that a single-phase region of β phase with ~1.5 μm in width can be formed adjacent to the Al matrix for all locations. Thus, the FC-VD plate has a similar thickness and structure of the diffusion layer with the FF plate.

3.4 Bonding strength and tensile properties

Figure 12 shows the shear strength of various plates along the RD. The shear strength of the FF plate is only 3.56 MPa, which is close to that of vacuum diffusion-bonded Mg/Al plates [49]. These results indicate that direct hot-pressing in the atmospheric environment can generate a bonding quality similar to vacuum diffusion bonding. FC plate exhibits far higher shear strength than FF plate. Clearly, the preparation of a corrugated interface can

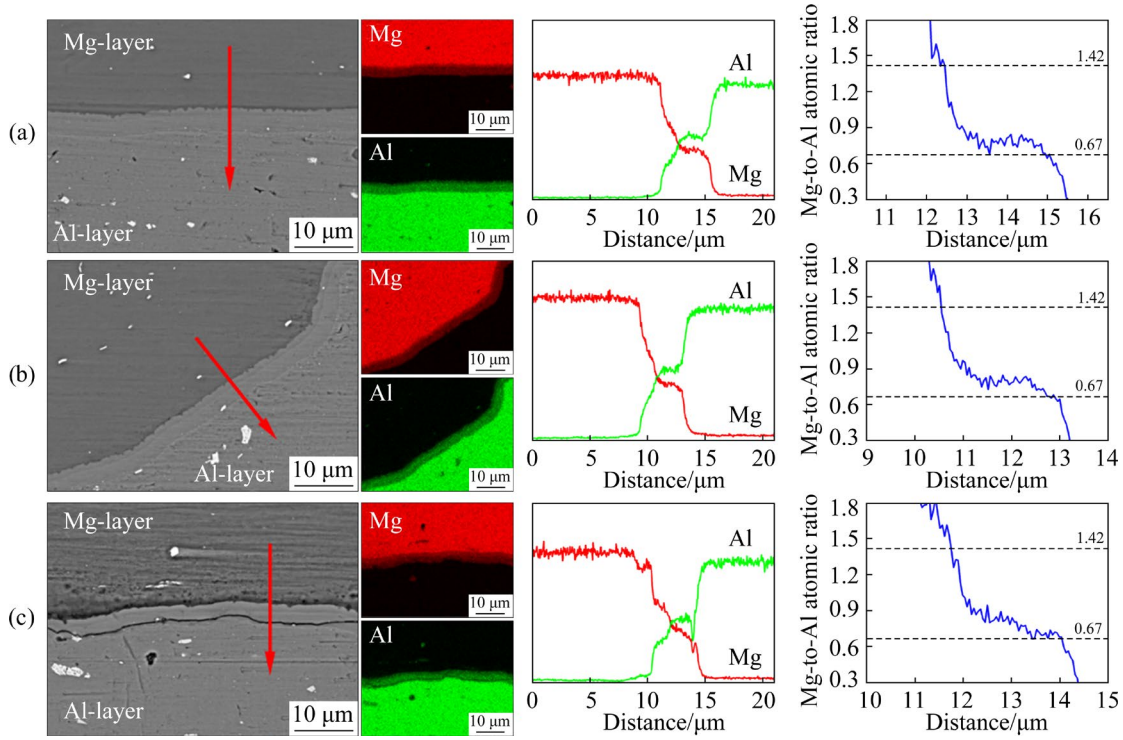

Fig. 11 SEM images and EDS mappings at different positions on ND−TD plane of FC-VD sample, element line-scanning spectra corresponding to red arrows in SEM images and Mg-to-Al atomic ratio in region of diffusion layer: (a) WP position; (b) WB-R position; (c) WV position

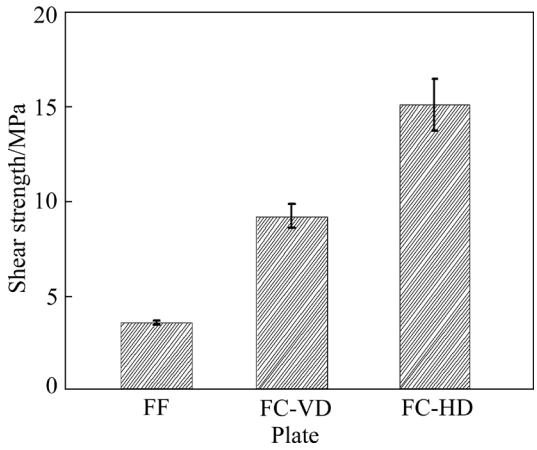

Fig. 12 Shear strengths of various plates along RD

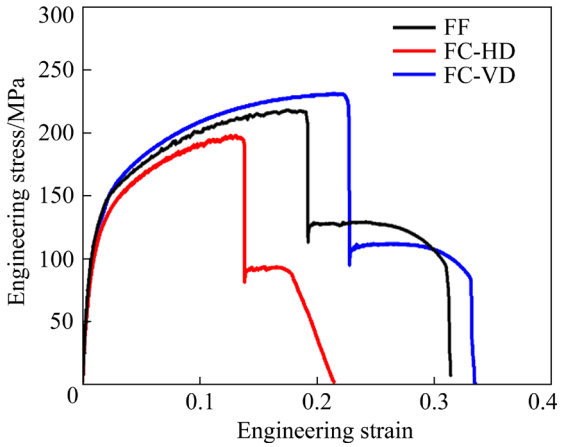

Fig. 13 Typical engineering stress−strain curves of various plates

greatly enhance the shear strength of the composite plates. The shear strength is largely dependent on the orientation relationship between shear direction and corrugated direction. The FC-HD plate exhibits a higher shear strength (15.09 MPa) than the FC-VD plate (8.29 MPa).

Figure 13 shows the tensile engineering stress−strain curve. The yield strength (σ_y) and peak strength (σ_p) are listed in Table 1. It is found that interface shape exhibits large influence on tensile properties. For the FF plate, the yield strength and peak strength are 119 and 214 MPa, respectively. The yield strength of the FC-VD plate (116 MPa) is close to that of the FF plate, while it is higher than

Table 1 Tensile properties of various plates

Plate	σ_y/MPa	σ_p/MPa	$\varepsilon_{f\text{-}1}$/%	$\varepsilon_{f\text{-}2}$/%
FF	119±3	214±3	18.9±0.4	30.0±1.4
FC-HD	102±1	195±4	13.5±0.5	21.1±0.4
FC-VD	116±4	231±1	21.0±3.0	31.2±3.5

that of the FC-HD plate (102 MPa). The corrugated interface can also influence peak strength. The FC-VD plate exhibits the highest peak strength (231 MPa). However, the peak strength of the FC-HD sample (195 MPa) is the lowest.

For three samples, two-step fracture behavior can be observed. The phenomenon has been reported for the Mg/Al composite plate [17]. The first fracture strain ($\varepsilon_{f\text{-}1}$) and second fracture strain ($\varepsilon_{f\text{-}2}$) are also measured and listed in Table 1. For the FF sample, $\varepsilon_{f\text{-}1}$ and $\varepsilon_{f\text{-}2}$ are 18.9% and 30.0%, respectively. In contrast, the FC-VD plate exhibits the highest $\varepsilon_{f\text{-}1}$ (21.0%) and $\varepsilon_{f\text{-}2}$ (31.2%), while the FC-HD plate has the lowest $\varepsilon_{f\text{-}1}$ (13.5%) and $\varepsilon_{f\text{-}2}$ (21.1%). Clearly, the mechanical properties of FC plates are also largely dependent on the orientation relationship between the corrugated direction at the interface and the stress axis.

4 Discussion

4.1 Influence of interface shape on microstructure

During hot-pressing at 350 °C, the dynamic recovery and dynamic recrystallization might be initiated, which could result in the decrease of KAM value and the nucleation of dynamic recrystallized grains. It is well known that the influence of thermal processing on the microstructure depends on the temperature, strain rate and strain amount [50]. For the present hot-pressing, the hot-pressing temperature is 350 °C, the strain rate is ~0.56 s^{-1} and the strain amount is ~40%. In AZ31 alloys, such deformation conditions can cause profuse dynamic recrystallization [51,52]. However, for the pure Al with high stacking fault energy, the defect density and recrystallization driving force significantly decrease as a result of the elevated dynamic recovery rates [53,54]. Thus, after hot-pressing, the elongated grains are remained in the Al matrix.

For AZ31 alloys, the deformation texture and recrystallization texture are similar [55]. And the refinement of grains via dynamic recrystallization can weaken the intensity of texture owing to the formation of many fine grains with different orientations [56]. Thus, for Mg layer, after hot-pressing, basal texture can be maintained, and the {0001} pole exhibits more scattered distribution, as shown in Fig. 4(a). For Al alloys, hot-pressing might enhance the R-cube texture owing to the suppression of the dynamic recrystallization [43]. However, a thickness reduction of 40% cannot also cause significant textural changes in Al alloys [57]. Thus, after hot-pressing, the cube {001}⟨100⟩ texture component is remained, as shown in Fig. 4(b). In general, the hot-pressing process exhibits less effect on the grain shape and texture of the FF plate with the flat interface.

Figures 7 and 9 indicate that the corrugated interface largely influences the grain shape and texture. For the Mg-layer, AFW, WP and WV positions in the FC plate exhibit a microstructure feature similar to the FF plate. The only difference is that the recrystallization level in the WV position is lower than in the other positions. It is reported that recrystallization level is dependent on temperature, strain rate and strain amount [58]. The WV position is the last point of contact between AZ31 and 1060 plates, and thus might suffer a low stress level and less strain than the other positions. This might be the reason why the WV position exhibits a low recrystallization level. Moreover, the corrugated interface can also influence the local texture component. The AFW, WP and WV positions still maintain basal texture component. However, for the WB position, the *c*-axis of texture is rotated towards the normal direction of interface, as shown in Fig. 7. For AZ31 alloys, the formation of texture is largely dependent on the stress state [47]. During hot compression or hot rolling at 350 °C, the *c*-axis of texture tends to rotate towards the compression axis [50,59]. This can be attributed to the fact that basal slip is the dominant deformation mechanism owing to its low critical resolved shear stress (CRSS) [60]. Thus, it is considered that the textural change can be mainly attributed to the change in stress state.

As shown in Fig. 14(a), for FF plate, the compressive stress is perpendicular to the flat interface. Thus, the Mg-layer in the FF plate still remains a strong basal texture component. For the FC plate, the compressive direction is also perpendicular to the interface, but it is constantly changed on the corrugated interface [59], as shown by the red arrow in Fig. 14(b). Thus, near the WB position, the corrugated interface in the FC plate causes the inclination of basal poles away from the ND towards the normal direction of the interface.

As discussed above, the present hot-pressing condition is hard to active profuse dynamic recrystallization and change the texture for the Al

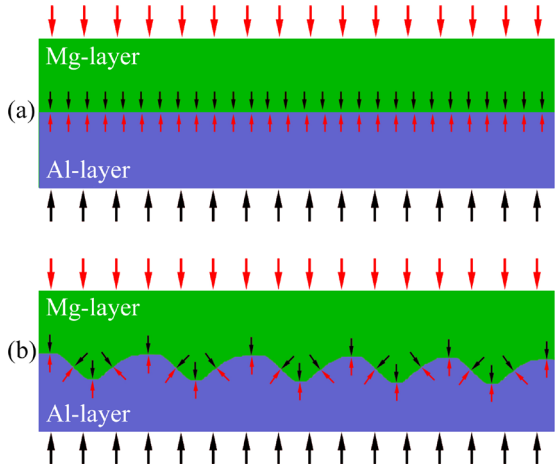

Fig. 14 Schematic diagram showing stress condition during hot-pressing: (a) FF plate; (b) FC plate (The red and black arrows represent the stress state applied to the Mg and Al layers, respectively)

substrate. However, for FC plates, hot-pressing can largely influence the local microstructure and texture at the interface of the Al substrate, as shown in Fig. 9. In this work, the Al plate with a corrugated surface was obtained by cold-pressing at room temperature. It is considered that severe plastic deformation might occur on the surface of the Al plate during cold-pressing. The influence of cold-pressing on microstructure of the Al substrate is shown in Fig. 15. During cold-pressing, the plastic strains are mainly concentrated near the contact surface. Therefore, cold-pressing has little influence on the microstructure of the AFW position in the FC plate, as shown in Figs. 9(a) and 15(a). Figures 15(b–d) indicate that cold-pressing can increase the KAM value of the locations near the corrugated surface. It is reported that the KAM value can be used to estimate the stored energy according to the energy of

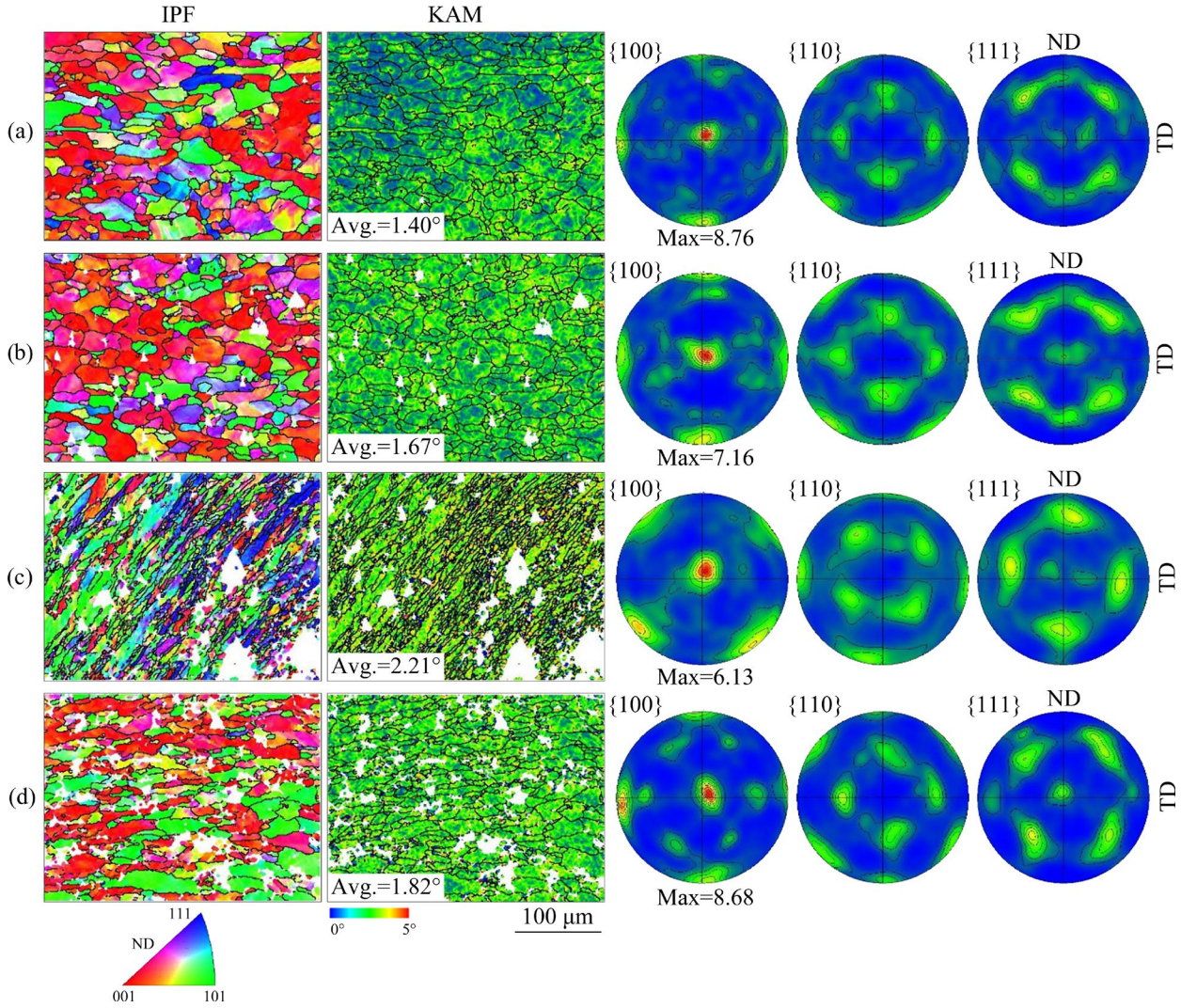

Fig. 15 EBSD maps and pole figures of various positions on Al plate subjected to cold-pressing: (a) AFW position; (b) WP position; (c) WB-R position; (d) WV position

geometrically necessary dislocations (GNDs) [61]. The stored energy can act as a driving force for the recrystallization [62]. Clearly, cold-pressing increases the stored energy, which promotes the occurrence of dynamic recrystallization during subsequent hot-pressing. Thus, after hot-pressing, the locations near the interface of the FC plate contain more equiaxed grains than the FF plate, as shown in Figs. 9(b−d). In particular, the WB position suffers the most intense plastic deformation at the interface, as shown in Fig. 15(c). The high KAM value largely enhances the dynamic recrystallization during hot-pressing, resulting in the formation of the equiaxed fine grains in the WB position of FC-plate, as shown in Fig. 9(c).

After cold-pressing, the WP, WV and AFW positions in the Al plate still retain the cube texture. However, the texture of the WB position generates a large change, as shown in Fig. 15(c). During deformation, texture evolution is largely dependent on the stress state. The WP, WV and AFW positions are mainly affected by compression stress along the ND. In contrast, the WV position produces the largest compression strain because it first contacts the mold. Clearly, present normal stress and strain cannot change the initial texture. For the WB position, strong local normal pressure and friction shear stress exist at the interface during cold-pressing [63]. In the corrugated rolling, it is also reported that the WB position has a higher equivalent strain than the WP and WV positions [63,64]. Similarly, the intense plastic strain might occur in the WB position during cold-pressing. The strong local normal pressure and friction shear stress exacerbate the elongation of grains and change the texture components. For the WB position of the FC-VD plate, the [001] axis rotates to the normal direction of corrugated surface around the RD, as shown in Fig. 15(c). As mentioned above, the high stored energy in the WB position can promote the recrystallization process during subsequent hot-pressing. Finally, the dynamic recrystallization texture is close to the deformation texture and exhibits more scattered distribution, as shown in Fig. 9(c).

4.2 Influences of interface shape on bonding strength

For laminate composite plates, maintaining the structural integrity is critical. If the interfacial delamination or debonding occurs during service, it can lead to total failure [65,66]. Thus, the interfacial bonding strength plays a vital role in assessing the overall quality of composite plates. The FF plate exhibits a very low shear strength value (only 3.56 MPa), as shown in Fig. 12. This value is similar to the vacuum diffusion welded Mg/Al composite plates [49]. Although the hot-pressing process is not protected by vacuum environment, plastic deformation has the ability to create fresh surfaces that facilitate metallurgical bonding of dissimilar metals in an atmospheric environment [48]. Plastic processing methods such as rolling and extrusion have gained the popularity for producing Mg/Al composite plates [28,32]. Achieving effective interfacial bonding requires a critical strain threshold. Research has indicated that a thickness reduction of 20% during rolling is necessary for AZ31/1060 composites [67]. To attain a successful metallurgical bonding at the Mg/Al interface, hot-pressing at 350 °C with a strain of 40% in an atmospheric environment has been proven to be effective, as shown in Figs. 10 and 11.

The bonding via the plastic processing is categorized as a solid-state bonding method [68]. There are two primary types of solid-state bonding: mechanical bonding and diffusion bonding [37]. The quality of metallurgical bonding is primarily determined by diffusion bonding. In the case of Mg/Al composite plates, the diffusion layer of the interface consists of a brittle reaction layer comprising the γ phase and β phase [69]. The reason for the low bonding strength in the FF plate can be ascribed to the formation of the brittle reaction layer at the Mg and Al interface [37].

For the FC plate, a similar diffusion layer is also formed at the interface, as shown in Fig. 11. It is reported that the diffusion layer thickness can influence the bonding strength. When the diffusion layer thickness exceeds 5 μm, there is a significant reduction in the interfacial bonding strength [37]. For the FF and FC samples, the thickness of the diffusion layer is comparable, as shown in Figs. 10 and 11. It is considered that the slight difference in diffusion layer thickness between the FC and FF plates cannot largely influence the bonding strength. However, the bonding strength of the FC-VD plate and the FC-HD plate is 2.3 times and 4.2 times that of the FF plate, respectively. The significant increase in bonding strength in the FC plate can be attributed

to another bonding mechanism: mechanical bonding [37]. This proves that the construction of a corrugated interface with a 3D structure can largely enhance the mechanical bonding effect. In contrast to a flat interface, a corrugated interface has a larger contact area and can create a robust "mechanical gearing" effect [41]. This effect is advantageous for strengthening the bonding strength at the interface. In order to exclude the effect of interface contract area on bonding strength, the modified shear strength is calculated as the ratio of maximum loading force to actual interfacial area. The values are listed in Table 2. It is shown that the modified shear strength of the FC plate is still far higher than that of the FF plate. The increasing shear strength can be attributed to the "mechanical gearing" effect via a corrugated interface [41].

Table 2 Modified shear strengths of various samples along RD (MPa)

FF	FC-VD	FC-HD
3.56	7.33	13.35

Interestingly, the modified shear strength of the FC-HD plate (13.35 MPa) is far higher than that of the FC-VD plate (7.33 MPa). This indicates that the "mechanical gear" effect on the FC-HD plate is higher than that on the FC-VD plate. This is related to the relationship between the loading direction and the corrugated direction. Compared with the flat interface in the FF plate, the corrugated interface in the FC-VD does not change the orientation relationship between the stress axis (the RD) and the interface (i.e., shear stress//interface), as shown in Fig. 1(d). Thus, it is considered that the "mechanical gear" effect might be not very high. However, for the FC-HD sample, the orientation of the interface with respect to the shear stress direction (the RD) is constantly changing, as shown in Fig. 1(c). In this case, the corrugated interface functions as a gear, facilitating the bonding of Mg and Al and exhibiting a substantial "mechanical gearing" effect [41]. As a result, the shear strength of the FC-HD plate greatly surpasses that of the FC-VD plate.

4.3 Influences of interface shape on tensile properties

Figure 13 shows that the corrugated interface can also influence the tensile property along the RD (e.g. yield strength and elongation). Compared with the FF plate, the FC-VD plate exhibits close yield strength, but the FC-HD sample has a lower yield strength. Clearly, the yield strength of the FC plate is also related to the orientation relationship between corrugated direction and tensile direction. It is well known that yield strength is largely dependent on the microstructure and texture of substrates [70]. As shown in Figs. 5, 7 and 9, the pre-corrugation treatment by cold-pressing can generate a large change in texture near the interface of Mg/Al composite plates. Although texture has little effect on yield strength of pure Al, it can significantly affect the yield strength of Mg alloys [71]. Based on the above results, Fig. 16 exhibits the schematic diagram showing the texture distribution near the interface of Mg/Al composite plates. For the FF plate, the Mg layer still contains strong basal texture (see Fig. 16(a)). When tension is applied along the RD, the tension direction is perpendicular to the *c*-axis. In such a scenario, the dominant deformation mechanism for the Mg layer is expected to be prismatic slip [72]. For the Mg layer of the FC plates, the *c*-axis of texture near the interface is usually perpendicular to the interface. For the WB position in the FC plates, the *c*-axis of texture is rotated to the normal direction of the corrugated interface during hot-pressing, as shown in Fig. 7. For the FC-HD plate, the *c*-axis of texture rotates towards the RD (~35°); however, for the FC-VD plate, the *c*-axis of texture rotates towards the TD (~35°), as shown in Figs. 16(b, c). Clearly, for the FC-VD plate, the

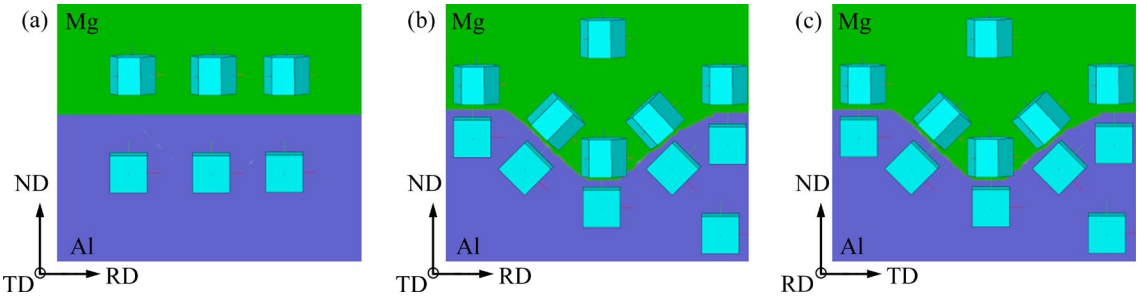

Fig. 16 Schematic diagram showing texture distribution near interface: (a) FF plate; (b) FC-HD plate; (c) FC-VD plate

c-axis of texture is still perpendicular to RD. Thus, it is considered that the change in texture has little influence on the tensile yield strength along the RD. However, for the WB position of the FC-HD plate, the *c*-axis of texture rotates ~35° towards the RD. This can largely enhance the activation of basal slip with the lowest CRSS [73]. This might be the reason why the FC-HD plate has a low yield strength.

Figure 13 indicates that the FF and FC plates exhibit two-step fracture behavior. In fact, such multi-step fracture behavior has been reported in the laminate composite plates [31,74]. This can be attributed to the significant difference in the elongation between constituents [31]. To interpret the fracture process, the macro-photographs of samples stretched to different strains are shown in Fig. 17. The strains corresponding to debonding (DB), fracture of Mg-layer (F-Mg) and fracture of Al-layer (F-Al) are labeled in the figures. Based on the results, the schematic diagrams of the tensile fracture process of Mg/Al plates are shown in Fig. 18. For all plates, the fracture process can be described as a two-step phenomenon, where the Mg layer and the Al layer undergo consecutive ruptures. After the Mg layer breaks during tension, the overall load-carrying capacity decreases, resulting in a sudden decrease in stress. It is reported that the interfacial bonding strength can also influence the fracture elongation [74]. When interfacial debonding occurs during service, the interface loses the transfer capacity of load-bearing. If the bonding strength is enhanced, the fracture strain of laminate composite plates can be improved by transferring the load-bearing responsibility from the relatively less ductile Mg-layer to the significantly more ductile Al-layer [74]. This might be the reason why the FC-VD plate exhibits higher fracture elongation than the FF plate. As shown in Fig. 17, the strain corresponding to debonding is 19% and 20% for the FF and FC-VD plates, respectively. The debonding and fracture of the Mg-layer occur almost simultaneously in the FF plate. In contrast, the fracture of the Mg layer is delayed by 4% strain compared to the debonding in the FC-VD plate. The delayed fracture strain of the Mg-layer might be related to the enhanced bonding strength. Unexpectedly, the FC-HD plate with the highest interfacial bonding strength exhibits the lowest fracture strain, as shown in Fig. 13. For the FC-HD plate, the strain corresponding to debonding is only 6%, resulting in the premature fracture of the Mg and Al layers, as shown in Fig. 17(b). It might be related to the orientation relationship between interface and loading force. For the FC-VD plate and FF plate, the loading force is parallel to the interface, as shown in Fig. 18(a). However, for the FC-HD plate, the orientation relationship between interface

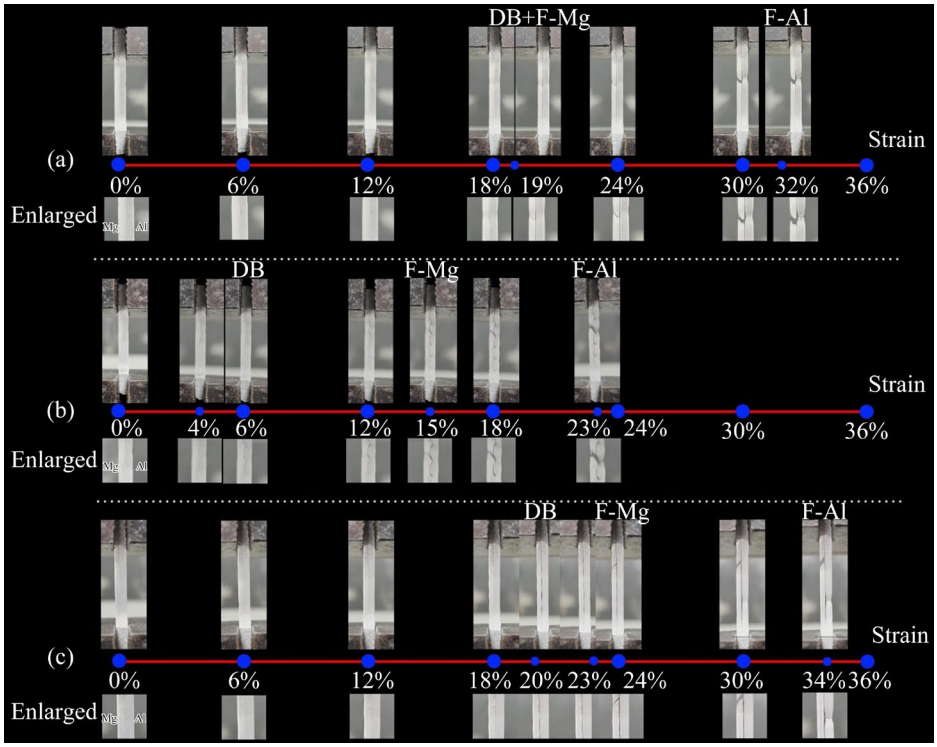

Fig. 17 Macro-photographs of plates stretched to different strains: (a) FF plate; (b) FC-HD plate; (c) FC-VD plate

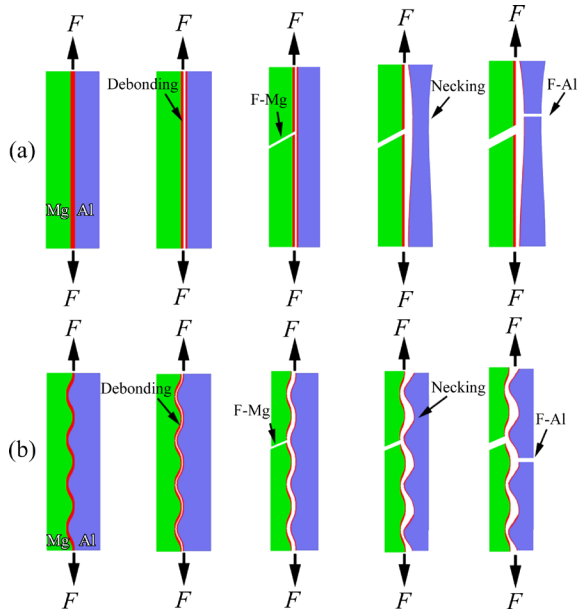

Fig. 18 Schematic diagrams of tensile fracture process of Mg/Al plates: (a) FF plate and FC-VD plate; (b) FC-HD plate

and loading force is constantly changed along the loading direction, as shown in Fig. 18. When the tensile stress axis is not parallel to the interface, a tensile stress component perpendicular to the interface is created, which can promote the occurrence of debonding. Corrugated interface leads to non-uniform distribution of the cross-section area in the tensile direction for the Al and Mg layers, as shown in Fig. 18(b). Thus, when the debonding once occurs, the positions with a small cross-section area become weak regions that are prone to premature necking and fracture. This might be the main reason why the FC-HD plate has very low debonding and fracture strains.

This study shows that the construction of the corrugated interface can greatly improve the interfacial bonding strength of Mg/Al LMCs. The results indicate that the Mg/Al LMCs with a corrugated interface show strong mechanical anisotropy. The existence of this anisotropy has an important impact on the forming and application of Mg−Al LMCs. In the further studies, it would be interesting to optimize the configuration of the 3D interface to further enhance the mechanical properties of the plates.

5 Conclusions

(1) A new method is proposed for preparing AZ31/1060 composite plates with the corrugated interface, which involves cold-pressing a corrugated surface in the Al plate and then hot-pressing the assembled Mg/Al plate.

(2) Hot-pressing with a thickness reduction of 40% in the atmospheric environment at 350 °C can cause significant element inter-diffusion and effective metallurgical bonding at the interface of Mg/Al composite plates. The diffusion layer thickness is ~5 μm which is similar to that of the Mg/Al composite plate prepared by hot rolling with reduction of 40% at 350 °C.

(3) For the FF plate, hot-pressing can cause profuse dynamic recrystallization on the Mg side, resulting in slight grain refinement and dispersion of basal texture. In contrast, hot-pressing exhibits little influence on the microstructure and texture of Al matrix. For the FC plates, the AFW position shows the similar change in microstructure to the FF plate.

(4) For the FC plates, severe plastic deformation occurring on the Al surface during the corrugation process promotes the dynamic recrystallization of the Al substrate near the interface during subsequent hot-pressing. Moreover, the initial corrugation on the surface of the Al plate changes the local stress state near the interface during hot-pressing, thereby altering the texture components of the substrates near the corrugated interface.

(5) The construction of the corrugated interface can greatly enhance the shear strength. And the mechanical properties of Mg/Al LMCs with corrugated interface are largely dependent on the orientation relationship between load direction and corrugated direction. Compared to the FF plate, the shear strengths of the FC-HD plate and the FC-VD plate are increased by ~320% and ~130%, respectively. The the FC-HD plate shows the highest shear strength, but exhibits the lowest fracture elongation among all samples.

CRediT authorship contribution statement

Shi-jun TAN: Experiments, Investigation, Writing − Original draft, Writing − Review & editing; **Bo SONG:** Conceptualization, Writing − Review & editing, Supervision, Project administration; **Hao-hua XU:** Experiments, Investigation, Writing − Original draft; **Ting-ting LIU:** Conceptualization, Writing − Review & editing, Supervision, Project administration; **Jia SHE:** Investigation, Writing − Review & editing; **Sheng-feng GUO:** Investigation, Writing − Review & editing; **Xian-**

hua CHEN: Investigation, Writing − Review & editing; **Kai-hong ZHENG:** Investigation, Writing − Review & editing, Project administration; **Fu-sheng PAN:** Investigation, Writing − Review & editing, Project administration.

Declaration of competing interest

The authors declare that they have no known competing financial interests or personal relationships that could have appeared to influence the work reported in this paper.

Data availability

Data will be made available on request.

Acknowledgments

This work was supported by Guangdong Major Project of Basic and Applied Basic Research, China (No. 2020B0301030006), Fundamental Research Funds for the Central Universities, China (No. SWU-XDJH202313), Chongqing Postdoctoral Science Foundation Funded Project, China (No. 2112012728014435) and the Chongqing Postgraduate Research and Innovation Project, China (No. CYS23197).

References

[1] LI Ting, WANG Tao, LIU Wen-wen, HUANG Zhi-quan, JIANG Zheng-yi, HUANG Qing-xue. Hot-rolling process and properties of large thickness ratio Al/Mg/Al laminates [J]. Transactions of Nonferrous Metals Society of China, 2023, 33: 3625−3640.

[2] GAO Hai-tao, KONG C, YU Hai-liang. Lightweight metal laminated plates produced via (hot, cold and cryogenic) roll bonding: A review [J]. Transactions of Nonferrous Metals Society of China, 2023, 33: 337−356.

[3] QIN Liang, FAN Min-yu, GUO Xun-zhong, TAO Jie. Plastic deformation behaviors of Ti−Al laminated composite fabricated by vacuum hot-pressing [J]. Vacuum, 2018, 155: 96−107.

[4] WU Yuan-bing, ZHAO Jian-hua, PENG Wei-li, GU Cheng, CHENG Jin, WANG Ya-jun. Optimization of additive manufactured Ti-based pyramidal lattice structure applied to interface strengthening of Mg/Ti bimetal composites [J]. Transactions of Nonferrous Metals Society of China, 2024, 34: 846−860.

[5] KUNČICKÁ L, KOCICH R. Optimizing electric conductivity of innovative Al−Cu laminated composites via thermo-mechanical treatment [J]. Materials & Design, 2022, 215: 110441.

[6] PENG H, CHEN D L, BAI X F, WANG P Q, LI D Y, JIANG X Q. Microstructure and mechanical properties of Mg-to-Al dissimilar welded joints with an Ag interlayer using ultrasonic spot welding [J]. Journal of Magnesium and Alloys, 2020, 8: 552−563.

[7] ZHU Cong-cong, XU Shi-wei, GAO Wen-li, MENG Yi-fan, LIN Sen, DAI Lu. Microstructure characteristics and mechanical properties of Al/Mg joints manufactured by magnetic pulse welding [J]. Journal of Magnesium and Alloys, 2023, 11: 2366−2375.

[8] HUO Peng-da, LI Feng, WANG Ye, XIAO Xing-mao. Formability and interface structure of Al/Mg/Al composite sheet rolled by hard-plate rolling (HPR) [J]. The International Journal of Advanced Manufacturing Technology, 2022, 118: 55−65.

[9] CHENG Qian, CHEN Liang, TANG Jian-wei, ZHAO Guo-qun, SUN Lu, ZHANG Cun-sheng. A comprehensive analysis on microstructure evolution of Mg−5.65Zn−0.66Zr alloy during hot deformation [J]. Journal of Magnesium and Alloys, 2021, 9: 520−531.

[10] KNAPEK M, ZEMKOVÁ M, GREŠ A, JABLONSKÁ E, LUKÁČ F, KRÁL R, BOHLEN J, MINÁRIK P. Corrosion and mechanical properties of a novel biomedical WN43 magnesium alloy prepared by spark plasma sintering [J]. Journal of Magnesium and Alloys, 2021, 9: 853−865.

[11] LI Chuan-qiang, HE Yi-bin, HUANG Huai-pei. Effect of lithium content on the mechanical and corrosion behaviors of HCP binary Mg−Li alloys [J]. Journal of Magnesium and Alloys, 2021, 9: 569−580.

[12] XIE Jin-shu, ZHANG Jing-huai, YOU Zi-hao, LIU Shu-juan, GUAN Kai, WU Rui-zhi, WANG Jun, FENG Jing. Towards developing Mg alloys with simultaneously improved strength and corrosion resistance via RE alloying [J]. Journal of Magnesium and Alloys, 2021, 9: 41−56.

[13] MANDAL P K, ROBI P S. Influence of micro-alloying with silver on microstructure and mechanical properties of Al−Cu alloy [J]. Materials Science and Engineering A, 2018, 722: 99−111.

[14] YUAN Liang-liang, GUO Ming-xing, HABRAKEN A M, DUCHENE L, ZHUANG Lin-zhong. Extremely improved formability of Al−Zn−Mg−Cu alloys via micro-domain heterogeneous structure [J]. Materials Science and Engineering A, 2022, 837: 142737.

[15] BAE J H, PRASADA RAO A K, KIM K H, KIM N J. Cladding of Mg alloy with Al by twin-roll casting [J]. Scripta Materialia, 2011, 64: 836−839.

[16] GUAN Feng, JIANG Wen-ming, LI Guang-yu, ZHU Jun-wen, WANG Jun-long, JIE Guo-liang, FAN Zi-tian. Effect of vibration on interfacial microstructure and mechanical properties of Mg/Al bimetal prepared by a novel compound casting [J]. Journal of Magnesium and Alloys, 2022, 10: 2296−2309.

[17] ZHANG Nan, WANG Wen-xian, CAO Xiao-qing, WU Jia-qi. The effect of annealing on the interface microstructure and mechanical characteristics of AZ31B/AA6061 composite plates fabricated by explosive welding [J]. Materials & Design (1980—2015), 2015, 65: 1100−1109.

[18] CHEN Zhi-qing, WANG Dong-ya, CAO Xiao-qing, YANG Wen-wu, WANG Wen-xian. Influence of multi-pass rolling and subsequent annealing on the interface microstructure and mechanical properties of the explosive welding Mg/Al composite plates [J]. Materials Science and Engineering A, 2018, 723: 97−108.

[19] ACARER M, DEMIR B, DIKICI B, SALUR E.

Microstructure, mechanical properties, and corrosion resistance of an explosively welded Mg–Al composite [J]. Journal of Magnesium and Alloys, 2022, 10: 1086−1095.

[20] GUO Yang-yang, QUAN Gao-feng, REN Ling-bao, LIU Bao-shuan, AL-EZZI S, PAN Hou-hong. Effect of Zn interlayer thickness on the microstructure and mechanical properties of two-step diffusion bonded joint of ZK60Mg and 5083Al [J]. Vacuum, 2019, 161: 353−360.

[21] YIN Fu-xing, LIU Can-chun, ZHANG Yong-guang, QIN Yan-fang, LIU Ning. Effect of Ni interlayer on characteristics of diffusion bonded Mg/Al joints [J]. Materials Science and Technology, 2018, 34: 1104−1111.

[22] JAFARIAN M, KHODABANDEH A, MANAFI S. Evaluation of diffusion welding of 6061 aluminum and AZ31 magnesium alloys without using an interlayer [J]. Materials & Design (1980—2015), 2015, 65: 160−164.

[23] ZHU Bo, LIANG Wei, LI Xian-rong. Interfacial microstructure, bonding strength and fracture of magnesium–aluminum laminated composite plates fabricated by direct hot pressing [J]. Materials Science and Engineering A, 2011, 528: 6584−6588.

[24] CAO Miao, WANG Cui-ju, DENG Kun-kun, NIE Kai-bo, LIANG Wei, WU Yu-cheng. Effect of interface on mechanical properties of Ti/Al/Mg/Al/Ti laminated composites [J]. Materials Research, 2020, 23: e20190648.

[25] HAN Ting-zhuang, ZOU Jing-feng, HUANG Guang-sheng, MA Li-feng, CHE Chao-jie, JIA Wei-tao, WANG Li-fei, PAN Fu-sheng. Improved strength and ductility of AZ31B Mg alloy sheets processed by accumulated extrusion bonding with artificial cooling [J]. Journal of Magnesium and Alloys, 2021, 9: 1715−1724.

[26] HAN Ting-zhuang, HUANG Guang-sheng, LI Heng, WANG Li-fei, ZHANG Hua, PAN Fu-sheng. Strength-ductility balance of AZ31 magnesium alloy via accumulated extrusion bonding combined with two-stage artificial cooling [J]. Journal of Magnesium and Alloys, 2023, 11: 1549−1555.

[27] TANG Jian-wei, CHEN Liang, ZHAO Guo-qun, ZHANG Cun-sheng, SUN Lu. Achieving three-layered Al/Mg/Al sheet via combining porthole die co-extrusion and hot forging [J]. Journal of Magnesium and Alloys, 2020, 8: 654−666.

[28] WU Yang, FENG Bo, XIN Yun-chang, HONG Rui, YU Hui-hui, LIU Qing. Microstructure and mechanical behavior of a Mg AZ31/Al 7050 laminate composite fabricated by extrusion [J]. Materials Science and Engineering A, 2015, 640: 454−459.

[29] XIN Yun-chang, HONG Rui, FENG Bo, YU Hui-hui, WU Yang, LIU Qing. Fabrication of Mg/AL multilayer plates using an accumulative extrusion bonding process [J]. Materials Science and Engineering A, 2015, 640: 210−216.

[30] SHENG Kun, LU Li-wei, XIANG Yao, MA Min, WU Zhi-qiang. Crack behavior in Mg/Al alloy thin sheet during hot compound extrusion [J]. Journal of Magnesium and Alloys, 2019, 7: 717−724.

[31] ZHANG X P, CASTAGNE S, YANG T H, GU C F, WANG J T. Entrance analysis of 7075 Al/Mg−Gd−Y−Zr/7075 Al laminated composite prepared by hot rolling and its mechanical properties [J]. Materials & Design, 2011, 32: 1152−1158.

[32] LUO Chang-zeng, LIANG Wei, CHEN Zhi-qiang, ZHANG Jian-jun, CHI Cheng-zhong, YANG Fu-qian. Effect of high temperature annealing and subsequent hot rolling on microstructural evolution at the bond-interface of Al/Mg/Al alloy laminated composites [J]. Materials Characterization, 2013, 84: 34−40.

[33] WANG Peng-ju, CHEN Ze-jun, HU Chao, LI Bo-xin, MO Tai-qian, LIU Qing. Effects of annealing on the interfacial structures and mechanical properties of hot roll bonded Al/Mg clad sheets [J]. Materials Science and Engineering A, 2020, 792: 139673.

[34] BENCHERIFA I, ABIB K, ABDEL YAZID K, ALILI B, BRADAI D. Corrosion behavior of Al/Mg/Al multilayered composite elaborated by accumulated roll bonding [J]. Transactions of Nonferrous Metals Society of China, 2024, 34: 122−138.

[35] CHOI D H, AHN B W, LEE C Y, YEON Y M, SONG K, JUNG S B. Formation of intermetallic compounds in Al and Mg alloy interface during friction stir spot welding [J]. Intermetallics, 2011, 19: 125−130.

[36] LIU Yang, MA Yun-zhu, LIU Wen-sheng, HUANG Yu-feng, WU Lei, WANG Tao, LIU Chao, YANG Lun. The mechanical properties and formation mechanism of Al/Mg composite interface prepared by spark plasma sintering under different sintering pressures [J]. Vacuum, 2020, 176: 109300.

[37] KIM J S, LEE K S, KWON Y N, LEE B-J, CHANG Y W, LEE S. Improvement of interfacial bonding strength in roll-bonded Mg/Al clad sheets through annealing and secondary rolling process [J]. Materials Science and Engineering A, 2015, 628: 1−10.

[38] WANG Yi-yu, LUO Guo-qiang, ZHANG Jian, SHEN Qiang, ZHANG Lian-meng. Microstructure and mechanical properties of diffusion-bonded Mg−Al joints using silver film as interlayer [J]. Materials Science and Engineering A, 2013, 559: 868−874.

[39] ZHANG Jian, LUO Guo-qiang, WANG Yi-yu, XIAO Yuan, SHEN Qiang, ZHANG Lian-meng. Effect of Al thin film and Ni foil interlayer on diffusion bonded Mg−Al dissimilar joints [J]. Journal of Alloys and Compounds, 2013, 556: 139−142.

[40] ZHANG Jian, SHEN Qiang, LUO Guo-qiang, WANG Yi-yu, LI Mei-juan, ZHANG Lian-meng. Microstructural characterization of the Mg/Cu/Al diffusion bonded joint [J]. Journal of Physics: Conference Series, 2013, 419: 012021.

[41] HUO Peng-da, LI Feng, WANG Ye, LI Chao. Corrugated interface structure and formation mechanism of Al/Mg/Al laminate rolled by hard plate [J]. Transactions of Nonferrous Metals Society of China, 2023, 33: 1038−1053.

[42] WANG Hong-wei WANG Cui-ju, DENG Kun-kun, NIE Kai-bo, LIANG Wei. Microstructure and mechanical properties of Al/Mg/Al composite sheets containing trapezoidal shaped intermediate layer [J]. Materials Science and Engineering A, 2021, 811: 140989.

[43] WANG Z J, ZHAI L, MA M, YUAN H, LIU W C. Microstructure, texture and mechanical properties of Al/Al laminated composites fabricated by hot rolling [J]. Materials Science and Engineering A, 2015, 644: 194−203.

[44] ALVI M H, CHEONG S W, SUNI J P, WEILAND H, ROLLETT A D. Cube texture in hot-rolled aluminum alloy 1050 (AA1050)—nucleation and growth behavior [J]. Acta Materialia, 2008, 56: 3098−3108.

[45] ZHAO K N, XU D X, LI H X, ZHANG J S, CHEN D L.

Microstructure and mechanical properties of Mg/Mg bimetal composites fabricated by hot-pressing diffusion and co-extrusion [J]. Materials Science and Engineering A, 2019, 764: 138194.

[46] BARRETT C D, IMANDOUST A, OPPEDAL A L, INAL K, TSCHOPP M A, EL KADIRI H. Effect of grain boundaries on texture formation during dynamic recrystallization of magnesium alloys [J]. Acta Materialia, 2017, 128: 270−283.

[47] AL-SAMMAN T, GOTTSTEIN G. Room temperature formability of a magnesium AZ31 alloy: Examining the role of texture on the deformation mechanisms [J]. Materials Science and Engineering A, 2008, 488: 406−414.

[48] BAY N. Cold welding. Part 1: Characteristics, bonding mechanisms, bond strength [J]. Metal Construction, 1986, 18: 369−372.

[49] LIU Wen-sheng, LONG Lu-ping, MA Yun-zhu, WU Lei. Microstructure evolution and mechanical properties of Mg/Al diffusion bonded joints [J]. Journal of Alloys and Compounds, 2015, 643: 34−39.

[50] XIN Ren-long, WANG Bing-shu, ZHOU Zheng, HUANG Guang-jie, LIU Qing. Effects of strain rate and temperature on microstructure and texture for AZ31 during uniaxial compression [J]. Transactions of Nonferrous Metals Society of China, 2010, 20: s594−s598.

[51] FATEMI-VARZANEH S M, ZAREI-HANZAKI A, BELADI H. Dynamic recrystallization in AZ31 magnesium alloy [J]. Materials Science and Engineering A, 2007, 456: 52−57.

[52] BHATTACHARYA R, LAN Y J, WYNNE B P, DAVIS B, RAINFORTH W M. Constitutive equations of flow stress of magnesium AZ31 under dynamically recrystallizing conditions [J]. Journal of Materials Processing Technology, 2014, 214: 1408−1417.

[53] WANG Qing, YANG Peng, ZHANG Bao-rui, FAN Hui, XU Xue-xia, LI Wen-bin, FAN Xiao-liang, WANG Jin-feng, DING Hai-min. Microstructure and texture evolution of cold rolled 1070 Al alloy during the subsequent annealing treatment [J]. Results in Physics, 2019, 13: 102178.

[54] GOURDET S, MONTHEILLET F. An experimental study of the recrystallization mechanism during hot deformation of aluminium [J]. Materials Science and Engineering A, 2000, 283: 274−288.

[55] DEL VALLE J A, RUANO O A. Influence of texture on dynamic recrystallization and deformation mechanisms in rolled or ECAPed AZ31 magnesium alloy [J]. Materials Science and Engineering A, 2008, 487: 473−480.

[56] JIANG M G, XU C, YAN H, FAN G H, NAKATA T, LAO C S, CHEN R S, KAMADO S, HAN E H, LU B H. Unveiling the formation of basal texture variations based on twinning and dynamic recrystallization in AZ31 magnesium alloy during extrusion [J]. Acta Materialia, 2018, 157: 53−71.

[57] REN B, MORRIS J G. Microstructure and texture evolution of Al during hot and cold rolling [J]. Metallurgical and Materials Transactions A, 1995, 26: 31−40.

[58] QUAN Guo-zheng, LI Gui-sheng, CHEN Tao, WANG Yi-xin, ZHANG Yan-wei, ZHOU Jie. Dynamic recrystallization kinetics of 42CrMo steel during compression at different temperatures and strain rates [J]. Materials Science and Engineering A, 2011, 528: 4643−4651.

[59] SUN Zheng, WU Yang, XIN Yun-chang, PENG Yan-shuo, FENG Bo, LIU Qing. Varying the strong basal texture in a Mg−3Al−1Zn plate by a new wave-shaped interface rolling [J]. Materials Letters, 2018, 213: 151−153.

[60] BOEHLERT C J, CHEN Z, GUTIÉRREZ-URRUTIA I, LLORCA J, PÉREZ-PRADO M T. In situ analysis of the tensile and tensile-creep deformation mechanisms in rolled AZ31 [J]. Acta Materialia, 2012, 60: 1889−1904.

[61] AZZEDDINE H, TIRSATINE K, BAUDIN T, MATHON M-H, HELBERT A-L, BRISSET F, BRADAI D. On the stored energy evolution after accumulative roll-bonding of invar alloy [J]. Materials Chemistry and Physics, 2017, 201: 408−415.

[62] MOHAMED G, BACROIX B. Role of stored energy in static recrystallization of cold rolled copper single and multicrystals [J]. Acta Materialia, 2000, 48: 3295−3302.

[63] GAO Xiang-yu, NIU Wen-quan, PEI Wen-le, HUANG Zhi-quan, WANG Tao, MA Li-feng. Deformation behavior and bonding properties of Cu/Al laminated composite plate by corrugated cold roll bonding [J]. Journal of Materials Research and Technology, 2023, 22: 3207−3217.

[64] GAO Xiang-yu, BIAN Li-ping, ZHAO Jing-wei, HAN Jian-chao, WANG Tao, HUANG Qing-xue. Interface-position-dependent structure evolution and mechanical behavior of corrugated cold rolled Cu/Al clad plate: experiment and simulation [J]. Journal of Materials Research and Technology, 2021, 13: 216−227.

[65] LIU Ting-ting, SONG Bo, HUANG Guang-sheng, JIANG Xian-quan, GUO Sheng-feng, ZHENG Kai-hong, PAN Fu-sheng. Preparation, structure and properties of Mg/Al laminated metal composites fabricated by roll-bonding, a review [J]. Journal of Magnesium and Alloys, 2022, 10: 2062−2093.

[66] LI Jian, FENG Bo, FENG Xiao-wei, CHEN Xian-hua, ZHENG Kai-hong, JIANG Xian-quan, PAN Fu-sheng Pan. Microstructure and mechanical behavior of Mg/Al composite plates with different thicknesses of Ti foil interlayer [J]. Journal of Magnesium and Alloys, 2024, https://doi.org/10.1016/j.jma.2024.07.008.

[67] LIU C Y, WANG Q, JIA Y Z, JING R, ZHANG B, MA M Z, LIU R P. Microstructures and mechanical properties of Mg/Mg and Mg/Al/Mg laminated composites prepared via warm roll bonding [J]. Materials Science and Engineering A, 2012, 556: 1−8.

[68] CAI W, DAEHN G, VIVEK A, LI J, KHAN H, MISHRA R S, KOMARASAMY M. A state-of-the-art review on solid-state metal joining [J]. Journal of Manufacturing Science and Engineering, 2019, 141: 031012.

[69] BRENNAN S, BERMUDEZ K, KULKARNI N S, SOHN Y. Interdiffusion in the Mg−Al System and Intrinsic Diffusion in β-Mg_2Al_3 [J]. Metallurgical and Materials Transactions A, 2012, 43: 4043−4052.

[70] WANG F, WILLIAMS S, COLEGROVE P, ANTONYSAMY A A. Microstructure and mechanical properties of wire and arc additive manufactured Ti−6Al−4V [J]. Metallurgical and Materials Transactions A, 2013, 44: 968−977.

[71] CHOI S H, BARLAT F, LIU J. Effect of precipitates on plastic anisotropy for polycrystalline aluminum alloys [J]. Metallurgical and Materials Transactions A, 2001, 32:

2239−2247.
[72] KOIKE J, OHYAMA R. Geometrical criterion for the activation of prismatic slip in AZ61 Mg alloy sheets deformed at room temperature [J]. Acta Materialia, 2005, 53: 1963−1972.
[73] AGNEW S R, DUYGULU Ö. Plastic anisotropy and the role of non-basal slip in magnesium alloy AZ31B [J]. International Journal of Plasticity, 2005, 21: 1161−1193.
[74] LEE K S, KIM J S, JO Y M, LEE S E, HEO J, CHANG Y W, LEE Y S. Interface-correlated deformation behavior of a stainless steel-Al−Mg 3-ply composite [J]. Materials Characterization, 2013, 75: 138−149.

界面形状对热压制造的镁铝复合板显微组织和力学性能的影响

谭世俊[1]，宋 波[1]，徐昊华[1]，刘婷婷[1]，佘 加[2]，郭胜锋[1]，陈先华[2]，郑开宏[3]，潘复生[2]

1. 西南大学 材料与能源学院，重庆 400715；
2. 重庆大学 材料科学与工程学院，重庆 400044；
3. 广东省科学院 新材料研究所，广州 510650

摘 要：提出了一种制备具有波形界面 AZ31/1060 复合板的新方法，即先在铝板上冷压波纹表面，然后将组装好的 Mg/Al 复合板进行热压复合。结果表明，冷压会在铝板波纹表面附近产生剧烈的塑性变形，在随后热压过程中促进界面附近铝基体动态再结晶的发生。此外，铝板表面的初始波纹会改变热压过程中界面附近的局部应力状态，从而对界面附近基体的织构组成产生较大的影响。波形界面的构建可以将剪切强度提高 2~4 倍，这主要归因于界面接触面积的增加和强的“机械咬合”效应。此外，复合板的力学性能在很大程度上取决于波纹方向与加载方向之间的取向关系。

关键词：Mg/Al 复合板；界面形状；显微组织；力学性能；织构

(Edited by Bing YANG)